INTERNATIONAL JOURNAL FOR NUMERICAL METHODS IN FLUIDS
Int. J. Numer. Meth. Fluids 2003; **43**:1045–1065 (DOI: 10.1002/fld.616)

Eulerian–Lagrangian DNS/LES of particle–turbulence interactions in wall-bounded flows

Luís M. Portela*,† and René V. A. Oliemans

Kramers Laboratorium voor Fysische Technologie, J. M. Burgerscentrum for Fluid Mechanics, Delft University of Technology, Prins Bernhardlaan 6, 2628 BW Delft, The Netherlands

SUMMARY

We developed a code for the direct numerical simulation of particle-laden turbulent flows, using the Eulerian–Lagrangian point-particle approach. The code uses a semi-implicit coupling scheme between the particles and the fluid, and a standard finite-volume single-phase solver, which can run either in DNS or LES mode; it can consider either one- or two-way coupling between the particles and the fluid. The code was used to study the dynamics of the particle–turbulence interactions in channel and pipe flows loaded with small, heavy particles. We present some results, from both an instantaneous-structure perspective (fluid turbulence structures and particle-concentration patterns), and a statistical perspective (probability distribution functions and correlations). Our results suggest that the near-wall particle–fluid interaction can be understood in terms of the interaction of the particles with the streamwise vortices. The strong streamwise vortices above the wall are responsible for the elongated streaky patterns that occur both in the deposition and resuspension of the particles. When two-way coupling is considered, the particles produce a large damping in the intensity of the streamwise vortices, without any significant change in their shape and their size. This damping leads to a weakening of the near-wall streaky-pattern, and to a reduction in the accumulation of particles at the wall. Copyright © 2003 John Wiley & Sons, Ltd.

KEY WORDS: particles; turbulence; wall-bounded flows; Eulerian–Lagrangian simulation; direct numerical simulation; large-eddy simulation

1. INTRODUCTION

Wall-bounded particle-laden turbulent flows are important in numerous industrial processes, such as: coal combustion, catalytic reactors, dust deposition and removal in clean rooms, droplets deposition in gas–liquid flows, etc. Of particular interest is the determination of the dispersion of the particles, and their deposition and resuspension at the walls, which depends on the particle–turbulence interaction.

*Correspondence to: L. M. Portela, Kramers Laboratorium voor Fysische Technologie, J. M. Burgerscentrum for Fluid Mechanics, Delft University of Technology, Prins Bernhardlaan 6, 2628 BW Delft, The Netherlands.
†E-mail: luis@klft.tn.tudelft.nl

Contract/grant sponsor: Dutch Foundation for Fundamental Research on Matter (FOM)

Received 1 April 2002
Revised 28 May 2003

A review of the early work on Eulerian–Lagrangian DNS/LES simulations of particle-laden turbulent flows can be found in Reference [1]. Most of the numerical work on the particle–turbulence interaction has been on homogeneous isotropic turbulence (e.g. References [2–4]). Besides the numerical work, there exists also some theoretical work on homogeneous isotropic turbulence. Starting from a postulated spectrum for the turbulence without particles, and using a force acting on the fluid to take into account the presence of the particles, Ooms and co-workers [5, 6] developed a model to predict the corresponding spectrum of the turbulence with particles.

The structure and dynamics of near-wall turbulence is very different from homogeneous isotropic turbulence, resulting in a different behaviour for both the particles and the turbulence. The interaction between the particles and the turbulence leads to a non-uniform particle concentration and the formation of particle clusters, which are quite different from the 'preferential concentration of particles' found in homogeneous isotropic turbulence [7]. Also, in wall-bounded flows the turbulence modification promoted by the particles is very different from homogeneous isotropic turbulence. For example, Kulick *et al.* [8] made measurements on the turbulence modification in a channel-flow of air laden with small heavy particles, and found that the degree of turbulence attenuation by the particles is much higher than in homogeneous isotropic turbulence.

We developed a code for the direct numerical simulation of particle-laden turbulent flows, using the Eulerian–Lagrangian approach, DELFT (Direct Eulerian–Lagrangian Flow Turbulence code). The code uses a semi-implicit coupling scheme between the particles and the fluid, and a standard finite-volume single-phase solver, which can run either in DNS (direct numerical simulation) or LES (large-eddy simulation) mode. The particles are assumed to be 'small' and are treated as point-particles. The code can consider either one-way coupling (i.e. neglect the modification of the flow by the particles) or two-way coupling (i.e. simultaneous calculation of both the forcing of the particles by the flow and of the flow by the particles).

We consider only the particle–turbulence interactions (either one- or two-way coupling), and neglect inter-particle interactions. When doing two-way coupling simulations, we deal with 'intermediate particle-loadings'. The assumption is that the particle concentration is high enough such that the turbulence modification by the particles is important, but low enough such that inter-particle interactions can be neglected. Note, however, that the local value of the particle concentration can be much higher than the average value; in particular, in regions where it occurs the formation of particle clusters. In these regions, inter-particle interactions might play an important role, even with quite small average values of the particle concentration.

DELFT was used to study channel and pipe fully developed turbulent flows loaded with small, heavy particles. We present some results from both an instantaneous structure perspective (fluid turbulence structures and particle-concentration patterns) and a statistical perspective (probability distribution functions and correlations). Our results suggest that both the particles deposition/resuspension and the influence of the particles on the turbulence can be understood in terms of the interaction of the particles with the streamwise vortices (the key turbulence-structure in single-phase wall-bounded flows [9, 10]).

The rest of the paper is organized as follows. In Sections 2 and 3 we present the formulation of the problem and the numerical method. In Section 4 we present the results for DNS of pipe flow with one-way coupling, focusing on the relation between the turbulence structure and the particles deposition and resuspension. In Section 5 we present the results for LES of channel

flow with two-way coupling, focusing on the turbulence modification by the particles. In Section 6 we summarize the major conclusions and offer some perspectives on the continuation of the work.

2. PROBLEM FORMULATION

The different coupling mechanisms that can occur in particle-laden flows are shown schematically in Figure 1. We consider an incompressible turbulent flow, where the flow and the particles are subject to some boundary and initial conditions. The flow exerts a force on the particles, which determines their trajectory. The particles exert an opposite force on the flow, producing a modification in the flow known as 'turbulence modulation'. If the particle mass-concentration is very small, then the influence of the particles on the flow can be neglected; this is known as one-way coupling. If the 'turbulence modulation' cannot be neglected, then the flow has to be solved simultaneously with the particle trajectories; this is known as two-way coupling. If the concentration of particles is high enough, then inter-particle interactions have also to be taken into account: inter-particle collisions and hydrodynamic coupling. Hydrodynamic coupling occurs when the distance between the particles is not large, when compared with the size of the particles, and the force acting on a particle depends on the position and velocity of the other particles. In this paper, we do not consider inter-particle collisions and hydrodynamic coupling.

In principle, the global initial and boundary conditions together with the boundary conditions imposed at the surface of each particle could be used to obtain a 'fully resolved simulation', with the detailed flow around every particle. Due to the large number of particles, this is impracticable with the computer resources available today. Instead of considering the detailed flow around every particle, the effect of the particles on the continuous phase is modelled, leading to modified equations for the continuous phase. These equations are solved using

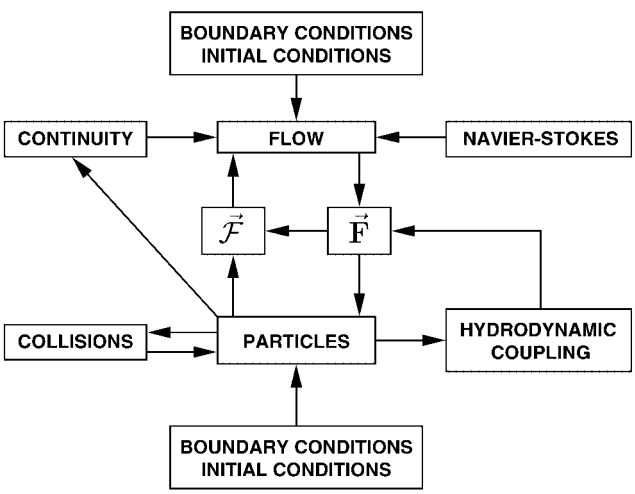

Figure 1. Coupling mechanisms in particle-laden flows.

numerical methods similar to the ones for single-phase flows (DNS, LES, etc.), together with the tracking of the individual particles. This is a standard approach when dealing with flows loaded with a large number of small particles, and it is usually called Eulerian–Lagrangian DNS (or LES). However, DNS is a misnomer, since the interaction between the particles and the fluid is modelled; it refers to the simulation of the continuous phase, which uses the Navier–Stokes equation together with an extra term to model the particle effects.

We are dealing with a very-small volume-fraction of particles, and the effect of the particles on the continuity equation can be neglected. The interaction between the particles and the fluid is felt through an exchange of momentum. The continuity and Navier–Stokes equations for the continuous phase become

$$\nabla \cdot \mathbf{U} = 0 \tag{1}$$

$$\rho \left\{ \frac{\partial \mathbf{U}}{\partial t} + (\nabla \mathbf{U}) \cdot \mathbf{U} \right\} = -\nabla P + \mu \nabla^2 \mathbf{U} + \mathscr{F} \tag{2}$$

where $\mathbf{U}$ is the velocity of the fluid (continuous phase), P is the pressure, ρ is the density, and μ is the viscosity. The continuity equation is exactly the same as for an incompressible flow without particles. The Navier–Stokes equation has the extra term $\mathscr{F}$, which is the force per unit of volume due to the particles. Equations (1) and (2) are solved together with the equations for the trajectory of the particles. For each particle we have

$$M \frac{\mathrm{d}\mathbf{V}}{\mathrm{d}t} = \mathbf{F} \tag{3}$$

where $\mathbf{V}$ is the velocity and M the mass of the particle. $\mathbf{F}$ is the force exerted by the fluid on the particle.

If the particle mass-concentration is very small, then $\mathscr{F}$ can be neglected in Equation (2). The continuity and Navier–Stokes equations become exactly the same as for the flow without particles, and Equations (2) and (3) are uncoupled. In addition to the solution of the single-phase flow, the problem simply requires the use of an algorithm for tracking the individual particles (one-way coupling). If $\mathscr{F}$ cannot be neglected in Equation (2), then Equations (1)–(3) need to be solved simultaneously (two-way coupling).

The solution of the problem depends on the models used for $\mathscr{F}$ and $\mathbf{F}$. We assume that the distance between the particles is large, when compared with the size of the particles, such that the force on a particle does not depend on the position and velocity of the other particles (i.e. we neglect hydrodynamic coupling). For small heavy particles in a gas, using order of magnitude estimates it can be shown that the most important force is the drag force (e.g. Reference [11]). Considering only the drag force:

$$\mathbf{F} = C_\mathrm{d} \left(\frac{\pi D_\mathrm{p}^2}{4} \right) \frac{\rho}{2} |(\mathbf{U}_\mathrm{p} - \mathbf{V})| (\mathbf{U}_\mathrm{p} - \mathbf{V}) \tag{4}$$

where D_p is the particle diameter, and $\mathbf{U}_\mathrm{p}$ is the velocity of the continuous-phase at the centre of the particle. For the drag coefficient C_d, similarly to Uijttewaal and Oliemans [12], we use a simple equation that gives a good approximation of the standard drag curve:

$$C_\mathrm{d} = \frac{24}{Re_\mathrm{p}} + 0.44 \tag{5}$$

where Re_p is the particle Reynolds number, defined as

$$Re_p \equiv \frac{|(\mathbf{U}_p - \mathbf{V})|D_p}{v} \tag{6}$$

where v is the kinematic viscosity of the fluid. For small values of Re_p, C_d reduces to $24/Re_p$, which is the drag coefficient in the case of Stokes drag. Here we consider only the drag force. However, the inclusion of other terms in the force exerted by the fluid on the particle, or the use of a different equation for the drag coefficient, is straightforward and it was done in other studies. For example, DELFT was used to study turbulent flows laden with small bubbles, considering the drag, buoyancy and added-mass forces [13].

In the case of two-way coupling, besides a model for $\mathbf{F}$, a model for $\mathscr{F}$ is needed. If the particles are much smaller than the smallest relevant length scale of the flow, then a simple point-particle approach is adequate. In this approach $\mathscr{F}$ is given by

$$\mathscr{F}(\mathbf{r}) = -\sum_{k=1}^{k=N_p} \mathbf{F}_k \delta(\mathbf{r} - \mathbf{P}_k) \tag{7}$$

where $\mathbf{r}$ is the position in the continuous phase, N_p is the total number of particles, $\mathbf{P}_k$ is the position of a particle, and $\mathbf{F}_k$ is the value of $\mathbf{F}$ for the particle at $\mathbf{P}_k$. $\delta(\mathbf{r} - \mathbf{P}_k)$ is a Dirac delta-function — i.e. the force of a particle on the fluid is considered applied at the point where the centre of the particle is located.

We use the point-particle approach, which imposes a severe restriction: the particle has to be significantly smaller than the grid-cell. The restriction comes from the fact that the velocity used to calculate the force on the particle, $\mathbf{U}_p$, is the velocity of the continuous phase at the centre of the particle. Since the particle is forcing the fluid, $\mathbf{U}_p$ itself is being influenced by the presence of the particle, and it is not the 'undisturbed fluid velocity', assumed in the standard point-particle derivation (e.g. Reference [14]). The 'local velocity disturbance', due to the particle presence, can be felt quite faraway from the particle. Since $\mathbf{U}_p$ is obtained by interpolating the fluid velocity in the neighbouring grid-points, this can result in a large underestimation of the particle–fluid force, unless the grid-cell is significantly larger than the particle.

There exist two opposing requirements: on one hand, the accuracy of the continuous-phase simulation requires a grid-cell significantly smaller than the fluid scales one wants to resolve, on the other hand, the point-particle approach requires a grid-cell significantly larger than the particle. If the particles are much smaller than the smallest relevant flow scales, then both requirements can be satisfied (assuming one has enough computer resources). However, in the so-called DNS point-particle approach, that would require particles much smaller than the Kolmogorov length-scale, which in most situations is not the case.

The restriction on the size of the grid-cell with respect to the size of the particles is associated with the basic assumptions of the point-particle approach, and it is applicable in both one-way and two-way coupling simulations. However, in two-way coupling simulations the violation of this restriction can lead to much more severe errors than in one-way coupling simulations.

When doing one-way coupling simulations, the surrounding fluid is not being disturbed by the particles, and the only consequence of using a small grid-cell is that the particles 'see' a local flow field with smaller scales than the ones that are forcing the actual particles.

Depending on the type of particle, this can introduce significant errors. However, for heavy particles in a gas, typically, the relaxation-time of the particles is significantly larger than the time scales of the small scales of the fluid. The particles are driven mostly by the large scales, and the error introduced by a small grid-cell is not as important as in two-way coupling simulations.

When doing two-way coupling simulations, the surrounding fluid, which is used to compute the force acting on the particle, is itself being disturbed by the particle. Unless the grid-cell is significantly larger than the particle, this can lead to large errors in the computation of both the trajectories of the particles and the effect of the particles on the turbulence [15]. An alternative, adopted in the channel-flow simulations with two-way coupling presented here, is to use a compromise solution: highly resolved LES calculations, using a grid-size that is able to resolve the most relevant turbulence structures, but it is still significantly larger than the particle size. This approach can be useful in numerous situations, like the one presented here, where the particles are smaller, but not much smaller, than the Kolmogorov length scale.

3. NUMERICAL METHOD

Currently, DELFT can deal with channel and pipe flows with periodic boundary conditions. Essentially, the codes for both geometries are similar, with the appropriate modifications due to the use of rectangular and cylindrical coordinates.

The numerical method per se is essentially the same, regardless of whether one uses DNS or LES; apart from a subgrid-scale (SGS) model in the case of LES. We use a finite-volume method on a staggered grid. For a finite-volume method, the interpretation of the point-particle approach is very natural. The method can be considered as a balance of momentum on a grid-cell, where, from the perspective of the continuous phase, the particles represent a source/sink of momentum. Since all the forces between the particle and the fluid occur at the surface of the particle, if we assume that a particle is either completely inside or completely outside of a grid-cell, then the source of momentum due to the particle is either equal to $-\mathbf{F}$ or equal to zero. Essentially, the numerical method consists of three parts: (i) continuous-phase solver, (ii) coupling between the continuous phase and the particles, and (iii) particle tracking.

3.1. Continuous-phase solver

The solution of the continuous phase uses a standard two-step predictor–corrector solver for single-phase incompressible flows (e.g. see Reference [16]). The flow is driven by a pressure gradient imposed along the streamwise direction, and we impose periodic boundary conditions both in the streamwise and spanwise directions. The Navier–Stokes equations are discretized using a second-order accurate method, and the time step is determined by the usual Courant stability criterion. In the predictor step, a provisional velocity is calculated without enforcing the continuity equation. In the corrector step, the continuity equation is enforced by means of a Poisson equation for the pressure. The Poisson equation is solved applying a fast Fourier transform in the two periodic directions, and solving tridiagonal matrices for the remaining direction. A more detailed description of the continuous-phase solver can be found in Reference [17].

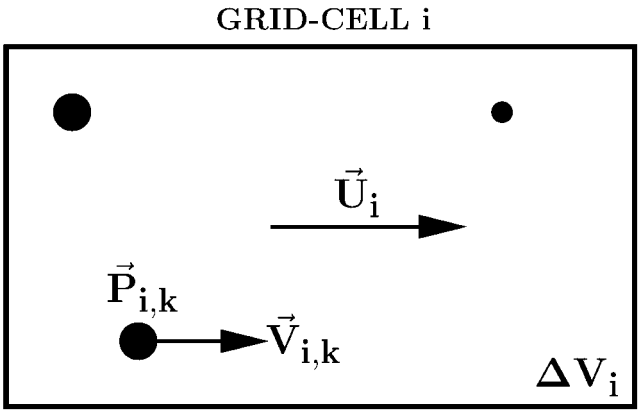

Figure 2. Computational grid-cell.

When doing a large-eddy simulation, an extra stress-tensor, $\mathbf{S}_s$, is introduced to represent the influence of the subgrid-scale motion on the resolved grid-scale velocities. Equation (2) becomes

$$\rho\left\{\frac{\partial \mathbf{U}}{\partial t}+(\nabla \mathbf{U})\cdot\mathbf{U}\right\}=-\nabla P+\mu\nabla^2\mathbf{U}+\nabla\cdot\mathbf{S}_s+\mathscr{F} \tag{8}$$

The value of $\mathbf{S}_s$ is determined using a subgrid-scale model. Here we use the standard Smagorinsky model, together with Van-Driest wall-damping (e.g. see Reference [16]).

3.2. Coupling scheme

We use the semi-implicit coupling scheme developed by Portela *et al.* [18], which has good numerical stability characteristics and is easy to parallelize. The basic idea is to first use the predictor part of continuous-phase solver to supply the value of $\partial\mathbf{U}/\partial t$ without $\mathscr{F}$. Then, use this value together with the models for $\mathscr{F}$ and $\mathbf{F}$ (Equations (4) and (7)) to solve simultaneously Equations (2) and (3), in order to obtain: the updated value of $\mathbf{V}$, and a new value of $\partial\mathbf{U}/\partial t$. The new value of $\partial\mathbf{U}/\partial t$ is used to update $\mathbf{U}$. Finally, use the corrector part of the continuous-phase solver to enforce the continuity equation.

Consider a grid cell i, with a volume ΔV_i and a fluid velocity $\mathbf{U}_i$, containing particles with masses $M_{i,k}$, at positions $\mathbf{P}_{i,k}$, with velocities $\mathbf{V}_{i,k}$ (Figure 2). At time step n, the predictor part of the continuous-phase solver provides the value of $\partial\mathbf{U}/\partial t$ without particles, $\partial\mathbf{U}_f/\partial t|_i^n$, which is combined with the force exerted by the fluid on each particle, $\mathbf{F}_{i,k}$, to give an equation for $\mathbf{U}_i^{n+1}$ and $\mathbf{V}_{i,k}^{n+1}$:

$$\mathbf{U}_i^{n+1}=\mathbf{U}_i^n+\left.\frac{\partial\mathbf{U}_f}{\partial t}\right|_i^n\Delta t-\frac{\Delta t}{\rho\Delta V_i}\sum_k\mathbf{F}_{i,k} \tag{9}$$

$$\mathbf{V}_{i,k}^{n+1}=\mathbf{V}_{i,k}^n+\frac{\Delta t}{M_{i,k}}\mathbf{F}_{i,k} \tag{10}$$

$$\mathbf{F}_{i,k}=\Phi(\mathbf{U}_i^n,\mathbf{U}_i^{n+1},\mathbf{V}_{i,k}^n,\mathbf{V}_{i,k}^{n+1}) \tag{11}$$

where Δt is the time-step interval. The function Φ is determined by the model for $\mathbf{F}$ and by the type of time advancement: explicit or implicit. In the case of implicit time-advancement we have a dependence on the values at time step $n+1$, whereas in the case of explicit time-advancement the dependence is only on the values at time step n. In order to obtain an explicit formula for $\mathbf{U}_i^{n+1}$, the function Φ is linearized. In the case of Stokes drag the function is already linear.

The provisional value of $\mathbf{U}_i^{n+1}$, given by Equation (9), is used to update the velocity of the continuous phase, and the corrector part of the continuous-phase solver is used to enforce the continuity equation, leading to a final value for $\mathbf{U}_i^{n+1}$.

For heavy particle-loading, the use of an implicit or semi-implicit coupling scheme is important, in order to avoid the severe restrictions on the value of the time step that occur in the case of an explicit coupling. These restrictions are imposed by numerical stability considerations. If numerical stability considerations do not impose a severe restriction, then an explicit coupling can be used. We tested several coupling and time-advancement schemes. For the simulations presented in this paper, with a moderate particle-loading, we found that an explicit time-advancement scheme could be used, without imposing more severe restrictions on the time step than the ones imposed by the Courant stability criterion of the continuous-phase solver. We used a second-order Adams–Bashforth time-advancement scheme, instead of the Euler time-advancement scheme explained above. The details are more involved, but the basic idea is the same.

3.3. Particle tracking

The particle tracking part updates the position of the particles, using the updated values of the velocities supplied by the coupling scheme. Essentially, this part is independent of the other two, and any standard tracking method can be used, with either an explicit or an implicit time-advancement scheme. The choice between implicit and explicit time-advancement will depend on the restrictions imposed on the time step by numerical stability considerations.

Typically, in Cartesian co-ordinates, explicit time-advancement requires a time interval smaller than the particle relaxation time. Here, we are dealing with heavy particles, with a relaxation time a few times larger than the time interval used by the continuous-phase solver (determined by the usual Courant stability criterion). Therefore, the use of explicit time-advancement does not pose numerical stability problems.

For the channel-flow geometry, we use a second-order Adams–Bashforth scheme. For the pipe-flow geometry, the continuous-phase solver uses cylindrical co-ordinates. However, the use of cylindrical co-ordinates for the particle tracking poses serious numerical stability problems near the centre of the pipe [19]. To solve this problem, in the pipe-flow geometry the particle tracking is done in Cartesian co-ordinates, together with a mapping between the Cartesian and the cylindrical co-ordinates. A more detailed description of the tracking algorithm for the pipe-flow geometry can be found in Reference [19].

When doing one-way coupling simulations, the coupling algorithm described above is not necessary. The equation of motion of the particles can be solved using the continuous-phase solver and an interpolation method to obtain the velocity of the continuous phase at the centre of the particle. Here, we use a standard tri-linear interpolation method.

4. DNS OF PIPE-FLOW WITH ONE-WAY COUPLING

We present the results of direct numerical simulations assuming elastic bouncing of the particles at the walls. The focus is on the relation between the turbulence structure and the particles deposition and resuspension. We consider only the drag force and use Equation (5) for the drag coefficient. Gravity was excluded, in order not to mix the gravitational effects with the particle–turbulence interaction. The inclusion of gravity is trivial (it simply requires the inclusion of the gravitational force in the equation of motion of the particle) and it was done in other studies using DELFT (e.g. Reference [19]).

The situation under consideration is sketched in Figure 3. The boundary conditions are periodic in the streamwise direction, and the streamwise length of the computational domain is $L_z = 5D$. We use cylindrical coordinates with 64 points in the radial direction, and 128 in the circumferential (spanwise) and streamwise directions. For the streamwise and circumferential directions we use a uniform grid spacing. For the radial direction we use a non-uniform grid spacing with an hyperbolic-tangent stretching: the smallest spacing at the wall ($\Delta r^+|_{\text{wall}} \approx 1.3$), and the largest spacing at the centre ($\Delta r^+|_{\text{centre}} \approx 4$).

The Reynolds number based on the wall-shear velocity $u_\tau \equiv \sqrt{\tau_w/\rho}$ (τ_w is the shear stress at the wall) and pipe diameter is equal to $Re_\tau = 360$, corresponding to a bulk Reynolds number $Re_b \approx 5300$, based on the mean fluid velocity in the pipe. The average values of the Kolmogorov length and time scales, L_k and T_k, can be estimated using the average dissipation rate of the turbulence kinetic energy:

$$L_k^+ \approx 1.6, \quad T_k^+ \approx 2.5 \tag{12}$$

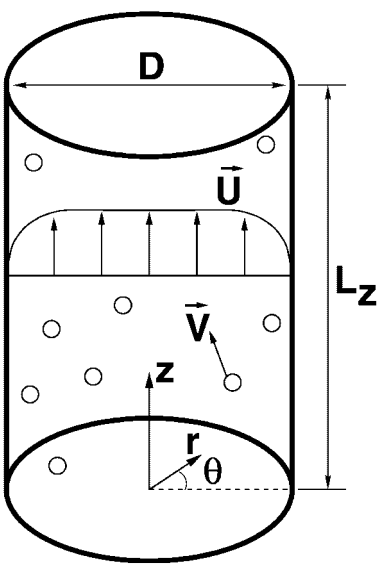

Figure 3. Particle-laden pipe flow.

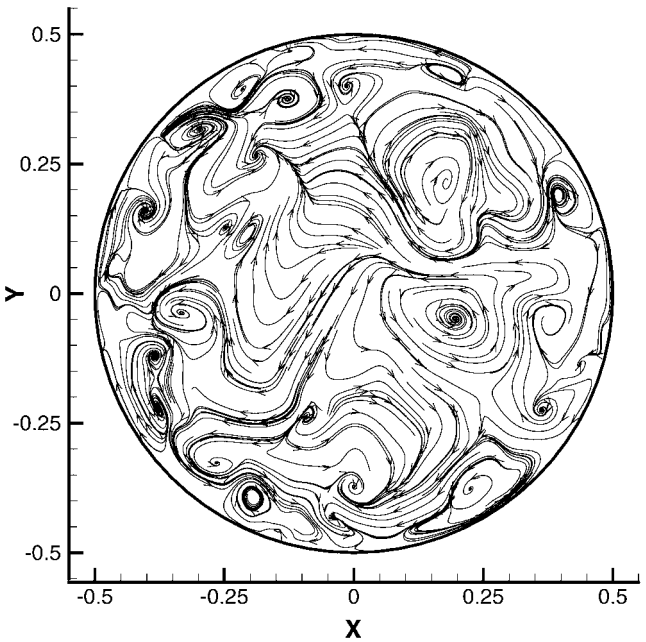

Figure 4. Instantaneous streamline pattern of the projection of the velocity field onto a plane perpendicular to the pipe axis.

Throughout this paper, the superscript $^+$ is used to represent a variable non-dimensionalised with wall variables; i.e. using u_τ and ν.

In Figure 4 we show a typical instantaneous streamline pattern of the projection of the velocity field onto a plane perpendicular to the streamwise direction. The pattern is very similar to the patterns occurring in a channel flow and in a flat plate turbulent boundary layer [20]. There exists an 'array of streamwise vortices' lying close to the wall. These streamwise vortices push high speed fluid towards the wall ('sweeps') and low speed fluid away from the wall ('ejections'). The streamwise vortices are the key structure to understand the near-wall turbulence dynamics, and are closely related with the well-known single-phase-flow streaky pattern near the wall, of alternating regions of low and high speed fluid [9, 10].

In order to get a better understanding of the interaction of the particles with the turbulence structure, and how it influences the particles deposition and resuspension, we performed two simulations:

1. uniform-start: random-uniform particle distribution over the entire pipe, with the initial particle velocity equal to the local fluid velocity.
2. wall-start: random-uniform distribution of the centre of the particles within a layer around the wall, with a thickness of one particle diameter, with the initial particle velocity equal to zero.

The uniform-start was used to study how the turbulence structure influences the particles dispersion and deposition. The wall-start was used to study how the turbulence structure

influences the particles resuspension. In both cases, the simulations are started without particles, which are introduced after a statistically steady state is reached. After their introduction, the number of particles remains constant during the entire simulation. When one particle leaves the domain, it is reintroduced with the same velocity at the opposite side. We used a total number of particles $N_p = 1.5 \times 10^5$, with the following characteristics:

$$\rho_p/\rho = 1000, \quad D_p^+ = 0.66, \quad T_p^+ = 25 \tag{13}$$

where ρ_p is the particle density, and T_p is the particle relaxation-time, defined as

$$T_p \equiv \frac{\rho_p}{\rho} \frac{D_p^2}{18\nu} \tag{14}$$

Since we use a non-uniform grid-spacing, the ratio between the grid-cell and particle sizes depends on the distance to the wall. Even though the particles are everywhere smaller than the grid-cells, the diameter of the particles is not everywhere 'much smaller' than the grid-spacing (e.g. close to the wall we have $D_p/\Delta r \approx 0.5$). In principle, this can introduce an error in the computation of the trajectories of the particles. However, since we are dealing with a one-way coupling situation, and the particle relaxation-time is significantly larger than the smallest time-scales of the flow ($T_p/T_k \approx 10$), we do not expect a large error associated with the small grid-spacing.

Note that the total number of particles is not a relevant physical parameter. We are dealing with a one-way coupling situation, which corresponds to the limit of a zero number of particles. A large number of particles was used simply for convenience in the visualization and statistics computation.

For the uniform-start, the time evolution of the distribution of the particles, in a slice of the pipe with a thickness equal to 1/20 of the pipe diameter, is shown in Figure 5, from shortly after the introduction of the particles ($t^+ = 14$) until $t^+ = 574$. For visualization purposes, the size of the particles is larger than the actual size.

The influence of the streamwise vortices on the particle dispersion and deposition is clear. In the core of the pipe the particles tend to cluster into the edge of circle-like patterns, with the central region nearly void of particles. The results suggest that: (i) the particle dispersion is not a simple gradient-diffusion phenomenon, and (ii) the particles tend to cluster at the edge of the streamwise vortices.

The clustering of the particles at the edge of the streamwise vortices has been observed by several authors (a review can be found in Reference [7]). It occurs for particles with an 'intermediate Stokes number' (the Stokes number is the ratio between the particle relaxation-time and a characteristic time scale of the flow). Very light particles behave as tracers, therefore they have a uniform concentration. Very heavy particles cannot respond to the vortices, during the time in which they are present. Eaton and Fessler [7] showed that an appropriate Stokes number to quantify the clustering of the particles at the edge of the vortices is

$$St_v \equiv \frac{T_p V_t}{R_v} \tag{15}$$

where R_v is the radius of the vortex, and V_t is the tangential velocity at the edge of the vortex. In wall-bounded flows, the size of the streamwise vortices depends on the distance to the wall [20]. The smaller vortices occur more frequently close to the wall, and the larger vortices

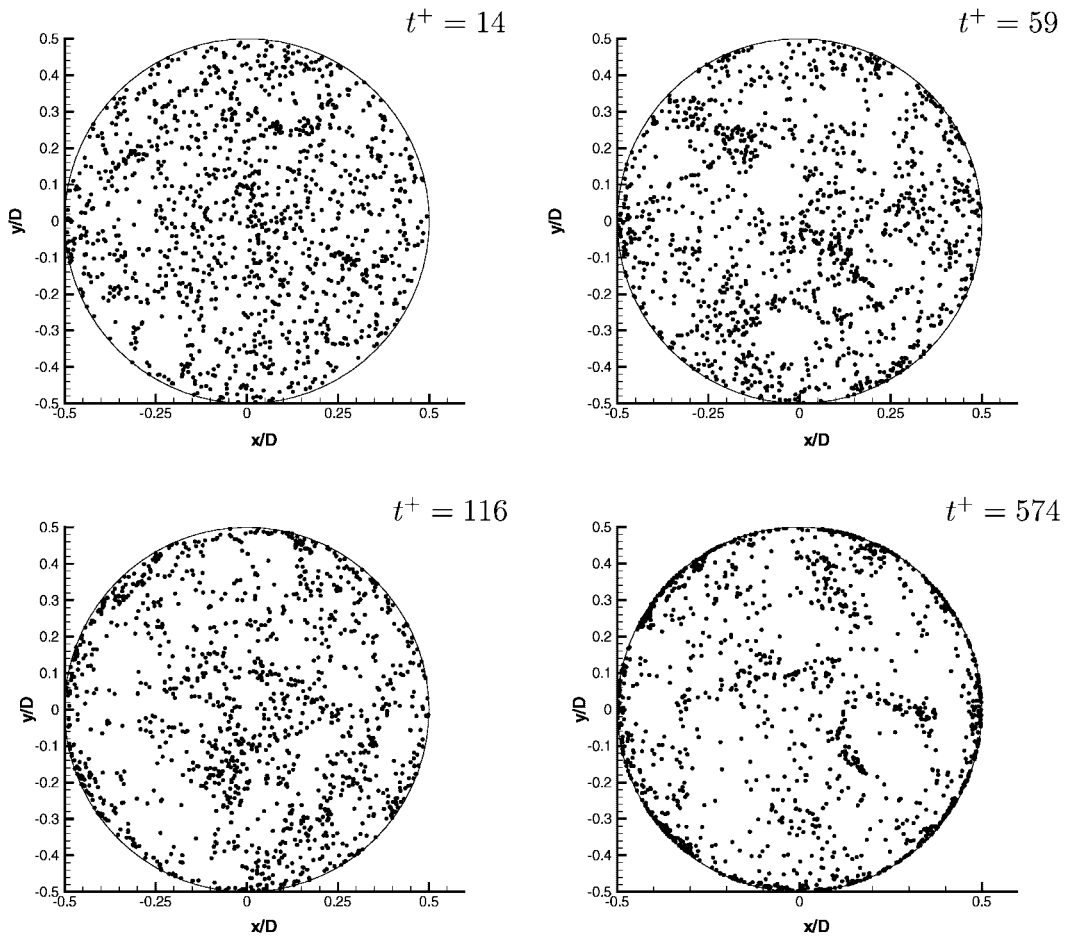

Figure 5. Time evolution of the distribution of the particles in a slice of the pipe with a thickness equal to 1/20 of the pipe diameter (uniform-start).

are found farther from the wall. In our case, the radius of the vortices is roughly between $R_v^+ \approx 10$ and $R_v^+ \approx 50$, with the smallest vortices occurring much more frequently close to the wall, and the largest vortices occurring almost exclusively in the central region of the pipe. Since the tangential velocity at the edge of the vortices is roughly $V_t^+ \approx 1$, the value of St_v is roughly between 0.5 and 2.5. This corresponds to the range of values where the clustering of the particles is expected to be more pronounced. According to Eaton and Fessler [7], the clustering of the particles at the edge of the vortices is most frequently observed when the value of St_v is between 0.1 and 1.

As time increases, the particles tend to accumulate near the wall, however, the near-wall particle concentration is not uniform. Very close to the wall the particles cluster into regions of high particle concentration, alternating with regions of low particle concentration. This pattern of alternating high–low concentration can be explained by the 'array of streamwise vortices'

lying close to the wall, pushing fluid towards the wall, hence pushing the particles towards the wall. This suggests that the mechanism responsible for the formation of the streaky pattern of high–low speed fluid close to the wall (the 'ejections' and 'sweeps' associated with the streamwise vortices) is also the main mechanism responsible for the particles deposition at the wall.

To visualize the particles resuspension in the wall-start case, it is convenient to unroll the pipe wall into a plane. Since the particles are located in a thin layer close to the wall, curvature effects are not important. The front and top views of the time evolution of the distribution of the particles in the wall-start case is shown in Figure 6, for the same time interval of the uniform start (from $t^+ = 14$ until 574). In the front view, the position of the particles is shown as a function of the angle along the wall (theta, in radians) and the distance to the wall (y^+, in wall units). In the top view, the position of the particles is shown as a function of the angle along the wall and the streamwise distance (zeta, normalized by the pipe diameter). For visualization purposes, in the top view the size and darkness of the particles was scaled according to the distance to the wall (being larger and darker farther from the wall).

The influence of the streamwise vortices on the particles resuspension is clear. The particles are resuspended according to a streaky pattern, somehow similar to the well-known single-phase-flow streaky pattern [9, 10]. The resuspension of the particles takes a relatively long time to occur, and it only starts to become apparent at $t^+ \approx 100$. At $t^+ = 574$ the streaky pattern formed by the resuspension of the particles is very clear. The spacing between the particle streaks is roughly 100 wall-units, which is also the well-known value of the single-phase-flow streak spacing. The relatively well-defined particle streaks, with roughly the same spacing of the single-phase-flow streak spacing, together with the relatively long time it takes for the particle streaks to be formed, suggests that the particle streaks are formed by strong streamwise vortices, as they travel along the wall in the streamwise direction. Essentially, this is the same mechanisms that has been proposed by several authors to explain the formation of the single-phase-flow streaky pattern [9, 10].

5. LES OF CHANNEL-FLOW WITH TWO-WAY COUPLING

We present the results of large-eddy simulations, assuming elastic bouncing of the particles at the walls and Stokes drag ($C_\mathrm{d} = 24/Re_\mathrm{p}$). Similarly to the pipe-flow simulations, we do not consider the gravitational force on the particles. The situation under consideration is sketched in Figure 7. The streamwise and spanwise lengths of the computational domain are: $L_x = 5H$ and $L_y = 2H$. Both in the streamwise and spanwise directions we used periodic boundary conditions and an uniform grid, with 64 grid points in each direction. In the direction normal to the walls we used 48 grid points, and a non-uniform grid-spacing with a power-function stretching: the smallest spacing at the wall ($\Delta z^+|_\mathrm{wall} \approx 4$), and the largest spacing at the centre ($\Delta z^+|_\mathrm{centre} \approx 13$).

The Reynolds number based on the wall-shear velocity and channel height is $Re_\tau = 500$, corresponding to a bulk Reynolds number $Re_\mathrm{b} \approx 8000$, based on the mean fluid-velocity in the channel. The average values of the Kolmogorov length and time scales are:

$$L_k^+ \approx 2.0, \quad T_k^+ \approx 4.0 \tag{16}$$

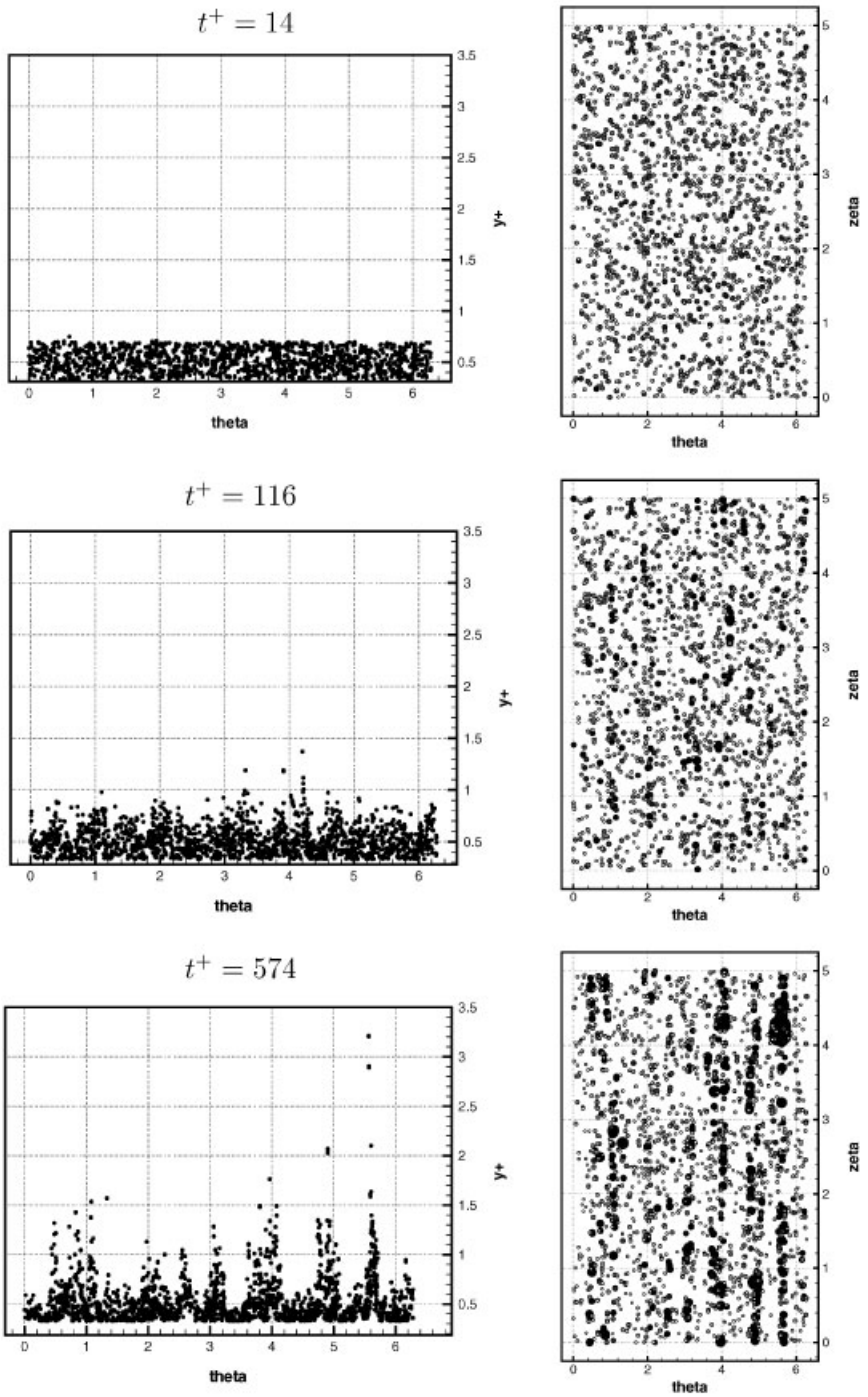

Figure 6. Time evolution of the distribution of the particles close to the pipe wall (wall-start); left: front view; right: top view.

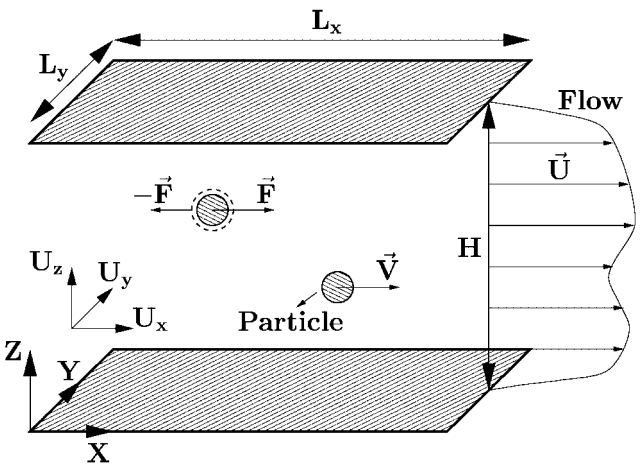

Figure 7. Particle-laden channel flow.

The simulations are started without particles. After a statistically steady state is reached, the particles are introduced in the flow with an initial velocity equal to zero. Similarly to the pipe-flow simulations, after their introduction, the number of particles remains constant during the entire simulation. The particles are introduced at 128 equally spaced positions in the streamwise direction, 64 in the spanwise direction and 48 in the normalwise direction, leading to a total number of particles $N_p = 393216$, with the following characteristics:

$$\rho_p/\rho = 8000, \quad D_p^+ = 0.5, \quad T_p^+ = 111 \tag{17}$$

Since we use a non-uniform grid-spacing, the ratio between the grid-cell and particle sizes depends on the distance to the wall. The smallest grid-cell occurs close to the wall, where we have: $\Delta x/D_p \approx 78$, $\Delta y/D_p \approx 31$, and $\Delta z/D_p \approx 8$. Therefore, in the entire channel, the grid-cells are significantly larger than the particles, and the error associated with the ratio between the grid-cell and particle sizes is small [15].

Contrary to the one-way coupling simulations, the number of particles is an important physical parameter of the problem, associated with the turbulence modification promoted by the particles. The number of particles corresponds to the following volume and mass fractions:

$$\phi_v \approx 2 \times 10^{-5}, \quad \phi_m \approx 0.16 \tag{18}$$

A few particle-relaxation-times after the introduction of the particles, a 'quasi-steady state' is reached. In the sense that the rate of particle accumulation at the walls remains approximately constant, and the changes in the fluid mean-velocity and turbulence are very small. Since the particles keep accumulating at the wall, the particle-concentration profile keeps changing, however, this change is very slow. Any changes in the fluid turbulence, which could occur as a result of the changes in the particle-concentration profile, are either very small, or very slow when compared to the turbulence time scales. The results shown here are at a time $t^* \approx 1$ ($t^* \equiv tu_\tau/H$) after the introduction of the particles, when this 'quasi-steady state' is already established ($t^* \approx 1$ corresponds to $t^+ \approx 500$, and it is approximately equal to five particle-relaxation times).

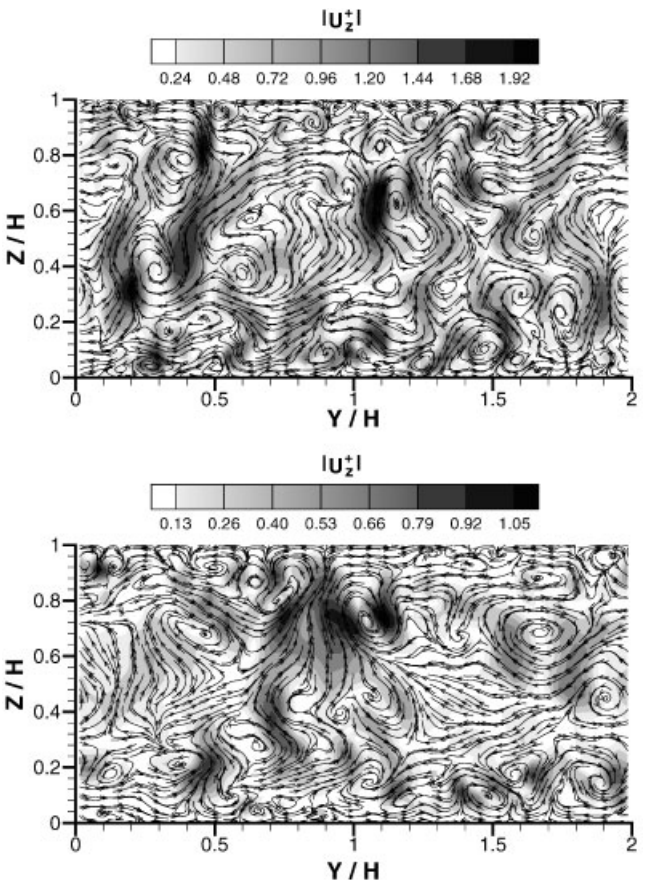

Figure 8. Streamlines of the projection of the instantaneous velocity field onto a plane perpendicular to the channel streamwise direction, and contours of the instantaneous absolute value of the normalwise velocity; top: unladen; bottom: particle-laden.

In Figure 8 we show two typical planes perpendicular to the streamwise direction (unladen and particle-laden), with the streamlines of the projection of the instantaneous velocity field onto the plane, and the contours of the instantaneous absolute value of the normalwise velocity. Comparing the unladen and particle-laden flow, it is clear that the particles produce a large decrease in the value of the normalwise velocity, damping the 'sweeps' and 'ejections' associated with the streamwise vortices. However, the shape and size of the streamwise vortices is not significantly changed by the particles.

In Figure 9 we show two typical streaky patterns (unladen and particle-laden) very close to the wall ($z^+ = 2$), in terms of: the contours of the value of the streamwise velocity, and the streamlines starting at 64 points uniformly distributed along $x = 0$. Clearly, without the particles the streaky pattern is better defined, more intense, and more wiggly, than for the particle-laden case. The effect of the particles on the streaky pattern can be understood in terms of the damping they produce on the intensity of the streamwise vortices, since the 'sweeps'

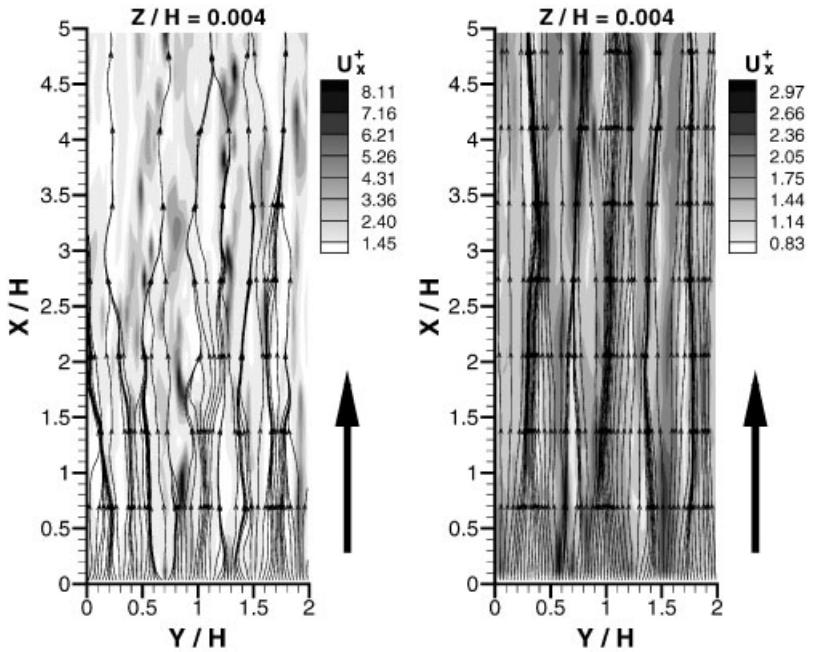

Figure 9. Instantaneous streaky patterns very close to the channel wall ($z^+ = 2$), in terms of the contours of the value of the streamwise velocity, and of the streamlines starting at 64 points uniformly distributed along $x = 0$; left: unladen; right: particle-laden.

and 'ejections' associated with the streamwise vortices are responsible for the streaky-pattern [9, 10].

In Figures 10 and 11, we show the probability distribution functions (PDF) of the normal and streamwise velocity fluctuations very close to the wall. For the normalwise velocity, the unladen PDF is roughly symmetric with respect to zero (negative values indicate a velocity towards the wall), and the particles produce a large decrease in both the negative and positive tails of the PDF, which remains roughly symmetric with respect to zero. For the streamwise velocity, the PDF is not symmetric with respect to zero: it has a shift towards negative values (negative mode), and a much larger tail for the positive values than for the negative values. This is a well-known characteristic of the streaky-pattern of alternating regions of low and high speed: the low speed streaks are larger and weaker, and the high speed regions are smaller and more intense. The particles make the PDF more symmetric with respect to zero: they shift the mode towards zero and produce a large decrease in the positive-values tail.

In Figures 12 and 13, we show the spanwise correlation of the normalwise velocity fluctuation and the streamwise correlation of the streamwise velocity fluctuation, of the fluid very close to the wall. The particles do not produce any significant change in the spanwise correlation of the normalwise velocity fluctuation, indicating that they do not produce any significant change in the size of the streamwise vortices. However, the particles produce a significant increase in the streamwise correlation of the streamwise velocity fluctuation, indicating a less wiggly streaky pattern.

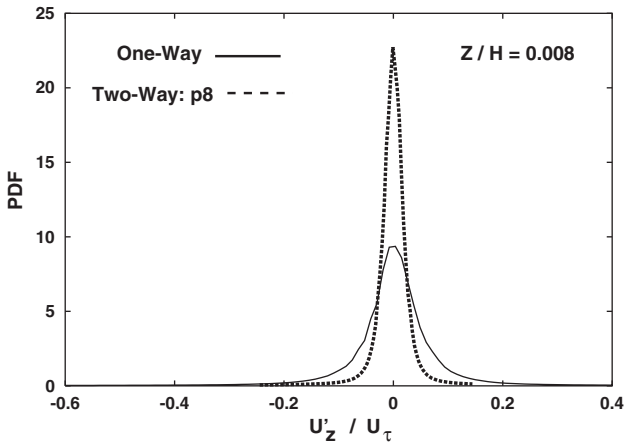

Figure 10. Probability distribution function of the normalwise velocity fluctuation of the fluid very close to the channel wall, at $z^+ = 4$ (negative values indicate a velocity towards the wall); —: unladen (one-way coupling); - - -: particle-laden (two-way coupling).

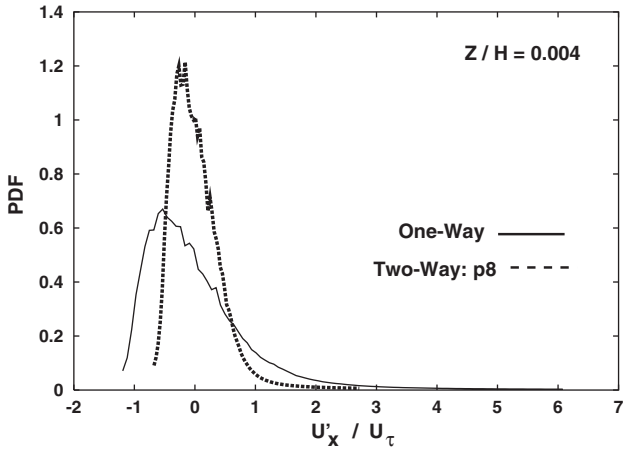

Figure 11. Probability distribution function of the streamwise velocity fluctuation of the fluid very close to the channel wall, at $z^+ = 2$; —: unladen (one-way coupling); - - -: particle-laden (two-way coupling).

From both an instantaneous-structure perspective (Figures 8 and 9) and a statistical perspective (Figures 10–13), it is clear that the main effect of the particles is to produce a large damping in the intensity of the streamwise vortices, without any significant change in their shape and size. This damping leads to a damping of the high-speed fluid pushed towards the wall, which in turn leads to a weakening of the streaky pattern.

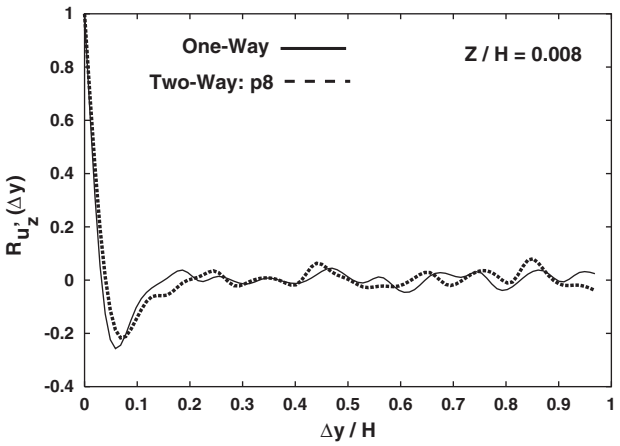

Figure 12. Spanwise correlation of the normalwise velocity fluctuation of the fluid very close to the channel wall, at $z^+ = 4$; —: unladen (one-way coupling); - - -: particle-laden (two-way coupling).

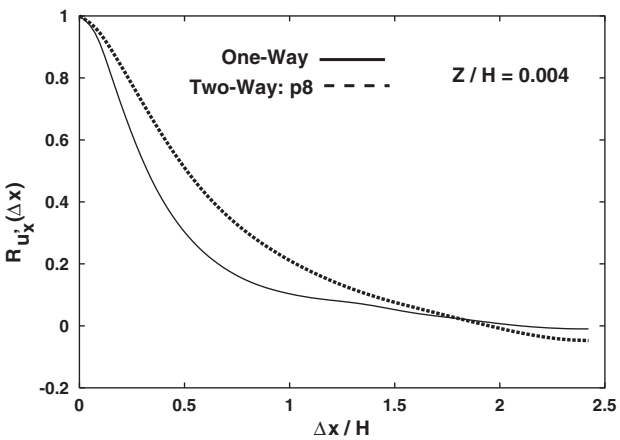

Figure 13. Streamwise correlation of the streamwise velocity fluctuation of the fluid very close to the channel wall, at $z^+ = 2$; —: unladen (one-way coupling); - - -: particle-laden (two-way coupling).

6. CONCLUSION

Our results suggest that the behaviour of wall-bounded particle-laden turbulent flows can be understood in terms of the interaction of the particles with the turbulence structure. Similarly to single-phase flows, streamwise vortices seem to be the key structure in particle-laden wall-bounded turbulent flows:

- Far from the wall the particles tend to cluster at the edge of the streamwise vortices, leading to the formation of circle-like patterns, with the central region nearly void of particles.

- The streamwise vortices push the particles towards the wall, leading to a high particle-concentration near the wall, with alternating regions of high-low particle-concentration.
- The streamwise vortices that travel above the wall in the streamwise direction seem to be responsible for most of the particle resuspension, which occurs not randomly, but according to a streaky pattern, somehow similar to the well-known streaky pattern of single-phase flows.

When two-way coupling effects are considered, the particles produce a large damping in the intensity of the streamwise vortices, without any significant change in their shape and size. This damping leads to the damping of the high-speed fluid pushed towards the wall, which in turn leads to the weakening of the streaky pattern. The weakening of the turbulence structure by the particles explains the smaller particle accumulation near the wall, observed by Portela *et al.* [21] in channel-flow simulations with two-way coupling.

The results presented here illustrate the usefulness of Eulerian–Lagrangian point-particle DNS/LES simulations to get a better understanding of the particle–turbulence interactions. We did not include inter-particle collisions, however, the inclusion of collisions is relatively simple, and it has been done in other studies [22]. A more severe limitation is related to the particle size: the particles have to be significantly smaller than the grid-cell. In two-way coupling simulations this restriction is particularly important, and highly-resolved LES may be more appropriate than DNS.

The results presented here illustrate that highly resolved LES calculations can be used to study the modification of the most relevant turbulence structures by the particles. We performed LES computations without any particle–fluid coupling at a subgrid-scale level. In our case we do not expect this to pose any significant problem, due to the following reasons: (i) we use a high-resolution LES, with a small amount of subgrid-scale turbulence kinetic energy, and (ii) we are dealing with moderate mass-fractions of small heavy particles (with a size smaller than the Kolmogorov length scale, and a relaxation-time much larger than the Kolmogorov time scale). However, for a lower resolution LES and/or different particles, a better subgrid-scale model might require the inclusion of one- and two-way coupling effects at a subgrid-scale level [23].

ACKNOWLEDGEMENTS

The continuous-phase solver for the channel and pipe flow geometries was developed by B. van Haarlem and J. Eggels, at the Laboratory for Aero and Hydrodynamics of the Delft University of Technology. The pipe flow results were obtained in collaboration with P. Cota. Computer resources were provided by the SARA Computing Center, in Amsterdam, and by the HPaC Computing Center of the Delft University of Technology. Financial support was provided by the Dutch Foundation for Fundamental Research on Matter (FOM), through its program on 'Dispersed Multiphase Flows'.

REFERENCES

1. McLaughlin JB. Numerical computation of particles-turbulence interaction. *International Journal of Multiphase Flow* 1994; (**Suppl.**)**20**:211–232.
2. Squires KD, Eaton JK. Particle response and turbulence modification in isotropic turbulence. *Physics of Fluids A* 1990; **2**(**7**):1191–1203.
3. Boivin M, Simonin O, Squires KD. Direct numerical simulation of turbulence modulation by particles in isotropic turbulence. *Journal of Fluid Mechanics* 1998; **375**:235–263.

4. Sundaram S, Collins LR. A numerical study of the modulation of isotropic turbulence by suspended particles. *Journal of Fluid Mechanics* 1999; **379**:105–143.
5. Ooms G, Jansen GH. Particles–turbulence interaction in stationary, homogeneous, isotropic turbulence. *International Journal of Multiphase Flow* 2000; **26**:1831–1850.
6. Ooms G, Gunning J, Poelma C, Westerweel J. On the influence of the particles-fluid interaction on the turbulent diffusion in a suspension. *International Journal of Multiphase Flow* 2002; **28**:177–197.
7. Eaton JK, Fessler JR. Preferential concentration of particles by turbulence. *International Journal of Multiphase Flow* 1994; (**Suppl.**)**20**:169–209.
8. Kulick JD, Fessler JR, Eaton JK. Particle response and turbulence modification in fully developed channel flow. *Journal of Fluid Mechanics* 1994; **277**:109–134.
9. Robinson SK. Coherent motions in the turbulent boundary layer. *Annual Review of Fluid Mechanics* 1991; **23**:601–639.
10. Kline SJ, Portela LM. A view of the structure of turbulent boundary layers. In *Self-Sustaining Mechanisms of Wall Turbulence*, Panton RL (ed.). Computational Mechanics Publications: Southampton, 1997; 167–180.
11. Michaelides EE. Review — the transient equation of motion for particles, bubbles and droplets. *Journal of Fluids Engineering* 1997; **119**:233–247.
12. Uijttewaal WSJ, Oliemans RVA. Particle dispersion and deposition in direct numerical and large eddy simulations of vertical pipe flows. *Physics of Fluids* 1996; **8**(**10**):2590–2604.
13. Portela LM, Ellepola JH, Oliemans RVA. Numerical study of the ratio between bubble and pressure driving-forces in upward bubbly turbulent pipe flows. *Proceedings of the Fourth International Conference on Multiphase Flow*, New Orleans, LA, U.S.A., May 27–June 1, 2001; 1–12.
14. Maxey MR, Riley JJ. Equation of motion for a small rigid sphere in a nonuniform flow. *Physics of Fluids* 1983; **26**(**4**):883–889.
15. Portela LM, Oliemans RVA. Direct and large-eddy simulation of particle-laden flows using the point-particle approach. In *Direct and Large-Eddy Simulation IV*, Geurts BJ, Friedrich R, Métais O (eds). Kluwer: Dordrecht, 2001; 453–460.
16. Ferziger JH, Perić M. *Computational Methods for Fluid Dynamics*; Springer: Berlin, 1996.
17. Eggels JGM. Direct and large eddy simulation of turbulent flow in a cylindrical pipe geometry. *Ph.D. Thesis*, Department of Mechanical Engineering, Delft University of Technology, Delft, 1994.
18. Portela LM, Oliemans RVA, Nieuwstadt FTM. Large-eddy simulation of particle-laden flows. In *Computational Fluid Dynamics 98*, Papailiou KD, Tsahalis D, Périaux JP, Knörzer D (eds), vol. 2. Wiley: Chichester, 1998; 292–299.
19. Cota P. Direct numerical simulation of horizontal particle-laden turbulent pipe flow. *Technical Report MEAH-187*, Department of Mechanical Engineering, Delft University of Technology, Delft, 1999.
20. Portela LM. Identification and characterization of vortices in the turbulent boundary layer. *Ph.D. Dissertation*, Department of Mechanical Engineering, Stanford University, Stanford, 1997.
21. Portela LM, Oliemans RVA, Nieuwstadt FTM. Numerical simulation of particle-laden channel flows with two-way coupling. *Proceedings of the Third ASME/JSME Joint Fluids Engineering Conference*, San Francisco, CA, USA, 18–23 July, 1999; 1–9; ASME paper FEDSM99-7890.
22. Li Y, McLaughlin JB, Kontomaris K, Portela L. Numerical simulation of particle-laden turbulent channel flow. *Physics of Fluids* 2001; **13**(**10**):2957–2967.
23. Portela LM, Oliemans RVA. Subgrid particle-fluid coupling evaluation in large-eddy simulations of particle-laden flows. *Proceedings of the ASME International Mechanical Engineering Conference and Exposition*, New Orleans, LA, USA, 17–22 November, 2002; 1–8; ASME paper IMECE2002-33113.

